A four-phase moving boundary problem in laser irradiation of amorphous silicon

R. Černý,[a] P. Přikryl[b]

[a]*Department of Physics, Faculty of Civil Engineering, Czech Technical University, Thákurova 7, 166 29 Prague 6, Czech Republic*

[b]*Mathematical Institute of the Academy of Sciences of the Czech Republic, Žitná 25, 115 67 Prague 1, Czech Republic*

Abstract

The phase transitions in thin layers of amorphous silicon on the quartz substrate caused by pulsed-laser irradiation are studied as a four-phase moving boundary problem with three moving boundaries using a nonequilibrium thermal model. Three phases, namely the liquid silicon (l-Si), the polycrystalline silicon (pc-Si), and amorphous silicon (a-Si) are treated explicitly, and the fourth phase, Si vapor, is included in the boundary conditions for l-Si. The numerical solution is performed using the Landau transformations, Galerkin finite element method and successive approximation approach with underrelaxation. In a practical application of the numerical model, the XeCl excimer laser irradiation of a-Si layers on quartz substrate is simulated. The effect of the numerical parameters of the model, of the pulse energy density and of the initial thickness of the a-Si layer is discussed.

1 Introduction

High quality polycrystalline silicon layers deposited onto inexpensive substrates have become an object of technological interest of electronics industry in recent years. Recrystallization of thin amorphous silicon layers due to light sources proved to be a very suitable method for preparing pc-Si, which is often used, e.g., as a metal gate in metal-oxide-semiconductor transistors [1]. Many theoretical and experimental studies have appeared dealing with the crystallization process of a-Si induced by pulsed-laser irradiation (e.g., [2–5]). In this paper, we present a computational model of pulsed-laser irra-

diation of an a-Si thin film which is based on the experimental work having been done before.

2 Physical model

In accordance with the results of the experimental work published in [2–5], we assume that the pulsed-laser induced phase changes in a-Si proceed as follows: The solid material is heated by the energy of the laser pulse until the surface reaches the temperature T_{ac}. Then, the solid-state crystallization of a-Si is initiated, resulting in the formation of pc-Si. The absorption of the pulse energy together with the release of the latent heat of a-Si $\rightarrow$ pc-Si transition leads relatively fast to the melting of the pc-Si surface and to the appearance of the liquid silicon. With a further temperature increase, also evaporation from the surface may become important [6].

After some time, the position of the l-Si/pc-Si interface reaches its maximum value due to the decrease of the absorbed laser energy. The melting process is then stopped and crystallization from the melt begins. Since the substrate is pc-Si previously recrystallized from a-Si, we can also assume that the product of the crystallization from the melt will be pc-Si. However, the grain size of the newly formed pc-Si may differ from that of the pc-Si substrate, since the process is running at a different temperature and velocity conditions at the interface than the previous a-Si $\rightarrow$ pc-Si transition. Therefore, the values of the thermal conductivity K_{pc} and of other thermophysical parameters may be different from those used before. Also, the latent heat of crystallization, L_{pc}, released during this process, and the equilibrium temperature of the l-Si $\rightarrow$ pc-Si transition, T_{pc}, need not generally be identical to the corresponding values, $L_{m,pc}$ and $T_{m,pc}$, for the melting process.

Finally, the l-Si/pc-Si interface reaches the surface and the crystallization is completed. As a result, the following sandwich structure of the sample can be formed. On the top, there are two pc-Si layers with possibly different grain sizes, localized on the remaining a-Si and the substrate (fused quartz, for instance).

3 Mathematical model

From the mathematical point of view, the described process can be classified as a four-phase moving boundary problem with three moving boundaries. Three phases, l-Si, pc-Si, and a-Si are treated explicitly, and the fourth phase, Si vapor, is included in the boundary conditions for l-Si. Supposing the one-dimensional heat conduction to be the dominant mode of energy transfer, we can write the energy balances in the form

$$\rho_i c_i \frac{\partial T_i}{\partial t} = \frac{\partial}{\partial x}\left(K_i \frac{\partial T_i}{\partial x}\right) + S_i(x,t), \quad i = pc, a, l, s, \tag{1}$$

where ρ is the density, c the specific heat, T the temperature, K the thermal conductivity, S the volume heating term due to the laser irradiation (see [6] for the exact form of this term), the indices pc, a, l are related to the polycrystalline, amorphous and liquid phases, resp., the index s means the substrate.

As in our previous work [6] we consider all phase changes to be nonequilibrium, which follows from the rapidity of the processes. Therefore, on every phase interface, we have one heat balance condition and one kinetic condition.

In the case of evaporation into vacuum, the conditions on the liquid/vapor interface (surface of the sample) can be expressed as follows:

$$\rho_l L_v \frac{\mathrm{d}Z_0}{\mathrm{d}t} = K_l \left(\frac{\partial T_l}{\partial x}\right)_{x=Z_0(t)_+} - \epsilon\sigma_{SB}(T_{Z_0}^4 - T_e^4), \tag{2}$$

$$\frac{\mathrm{d}Z_0}{\mathrm{d}t} = \frac{F}{\rho_l}\sqrt{\frac{M}{2\pi R_g}}\, T_{Z_0}^C \cdot 10^{-(A/T_{Z_0})+B}, \tag{3}$$

where Z_0 is the position of the liquid/vapor interface, ϵ the emissivity from the liquid surface, σ_{SB} the Stefan-Boltzmann constant, T_{Z_0} the temperature of the liquid/vapor interface, L_v the latent heat of evaporation, M the molar mass, R_g the universal gas constant, T_e the temperature of the surroundings, i.e., in $x \to -\infty$, A, B, C, F are constants (see [6], for details).

On the pc-Si/l-Si interface we have

$$\rho_{pc} L_{m,pc} \frac{\mathrm{d}Z_1}{\mathrm{d}t} = K_{pc}\left(\frac{\partial T_{pc}}{\partial x}\right)_{x=Z_1(t)_+} - K_l\left(\frac{\partial T_l}{\partial x}\right)_{x=Z_1(t)_-}, \tag{4}$$

$$\frac{\mathrm{d}Z_1}{\mathrm{d}t} = F_1(T_{Z_1} - T_{m,pc}), \tag{5}$$

where $L_{m,pc} = L_{m,a} + L_{a,pc}$ is the latent heat of melting of pc-Si, $L_{m,a}$ is the latent heat of melting of amorphous silicon, $L_{a,pc}$ the latent heat of the a-Si $\to$ pc-Si transition, Z_1 the position of the pc-Si/l-Si interface, F_1 is a constant [7].

Finally, on the pc-Si/a-Si interface we can write

$$\rho_a L_{a,pc} \frac{\mathrm{d}Z_2}{\mathrm{d}t} = K_{pc}\left(\frac{\partial T_{pc}}{\partial x}\right)_{x=Z_2(t)_-} - K_a\left(\frac{\partial T_a}{\partial x}\right)_{x=Z_2(t)_+}, \tag{6}$$

$$\frac{\mathrm{d}Z_2}{\mathrm{d}t} = F_2(T_{Z_2} - T_{ac}), \tag{7}$$

where Z_2 is the position of the pc-Si/a-Si interface, F_2 is a constant [7], the pc-Si/a-Si interface velocity $\mathrm{d}Z_2/\mathrm{d}t$ is assumed to be always positive since the reverse transition pc-Si $\to$ a-Si is not considered.

The other boundary conditions and the initial conditions have the form

$$\frac{\partial T}{\partial x}(D, t) = 0, \tag{8}$$

$$T(x,0) = T_0 = \text{const.}, \quad x \in [0, D], \tag{9}$$

$$Z_0(0) = Z_1(0) = Z_2(0) = 0, \tag{10}$$

where D is the thickness of the sample.

4 Numerical solution

First, we use the Landau transformations to map the domains occupied by the particular phases onto fixed space intervals $\xi \in [0,1]$. We thus write

$$\xi = \frac{x - Z_0(t)}{Z_1(t) - Z_0(t)}, \quad x \in [Z_0(t), Z_1(t)], \tag{11}$$

in the liquid and employ similar transformations in the other phases.

Equation (1) is then for the liquid phase transformed into

$$(Z_1 - Z_0)\rho_l c_l \frac{\partial T_l}{\partial t} - \rho_l c_l \left[\xi \frac{\mathrm{d}Z_1}{\mathrm{d}t} + (1-\xi)\frac{\mathrm{d}Z_0}{\mathrm{d}t}\right] \frac{\partial T_l}{\partial \xi} = \frac{1}{Z_1 - Z_0} \frac{\partial}{\partial \xi}\left(K_l \frac{\partial T_l}{\partial \xi}\right) + \\ + (Z_1 - Z_0) S_l(\xi, t), \tag{12}$$

and for the other phases transforms analogously. The interface conditions (2), (4), (6) change their form accordingly. The other equations are not changed, only in (8) and (9) D has to be replaced by 1, and x by ξ.

To solve the fixed-domain initial-boundary value problem obtained after transformations we employ the Galerkin finite element method. We approximate the temperature field in each finite element by $T \approx \langle N \rangle^e \{T\}^e$, where $\langle N \rangle^e$ is the row vector of linear basis functions on the element and $\{T\}^e$ is the column vector of the nodal values of temperature. Note that we use the standard FEM notation $\langle \cdot \rangle$, $\{\cdot\}$ for the row and column vectors and denote square matrices by square brackets, $[\cdot]$.

Performing the localization of the element matrices and vectors into the global ones we use conditions (4), (6) for coupling the global matrices of the individual phases and the condition (2) as a Neumann condition at $\xi = 0$ in the liquid phase. The condition (8) is then processed as a Neumann condition at $\xi = 1$ in the substrate. Conditions (3), (5) and (7) are used in the iteration procedure described later.

The space discretization leads to a system of ordinary differential equations for $\{T\}$, which is then subject of discretization in time. Supposing now that the initial state $\{T\}_t$ is known, we get a system of nonlinear algebraic equations for $\{T\}_{t+\Delta t}$ which can be schematically expressed as

$$[H(Z_0, \dot{Z}_0, Z_1, \dot{Z}_1, Z_2, \dot{Z}_2)]\{T\}_{t+\Delta t} = \\ [P(Z_0, \dot{Z}_0, Z_1, \dot{Z}_1, Z_2, \dot{Z}_2)]\{T\}_t - \{U(Z_0, Z_1, Z_2)\} - \{B(\dot{Z}_0, \dot{Z}_1, \dot{Z}_2)\}, \tag{13}$$

where the vector $\{U\}$ contains the volume source terms, $\{B\}$ represents the boundary conditions, and the dots denote time derivatives.

To proceed with the solution from time t to $t + \Delta t$ we have to solve the system of equations (13), (3), (5), (7). We use the following iteration algorithm in each time step:

1. Put $Z_1^{(1)}(t+\Delta t) = Z_1(t)$, $\dot{Z}_1^{(1)}(t+\Delta t) = \dot{Z}_1(t)$, $Z_2^{(1)}(t+\Delta t) = Z_2(t)$, $\dot{Z}_2^{(1)}(t+\Delta t) = \dot{Z}_2(t)$, $Z_0^{(1)}(t+\Delta t) = Z_0(t)$, $\dot{Z}_0^{(1)}(t+\Delta t) = \dot{Z}_0(t)$.
2. Compute $\{T\}_{t+\Delta t}^{(1)}$ from (13) using $Z_1^{(1)}(t+\Delta t)$, $\dot{Z}_1^{(1)}(t+\Delta t)$, $Z_2^{(1)}(t+\Delta t)$, $\dot{Z}_2^{(1)}(t+\Delta t)$, $Z_0^{(1)}(t+\Delta t)$, $\dot{Z}_0^{(1)}(t+\Delta t)$.
3. Compute $\dot{Z}_1^{(2)}(t+\Delta t)$ from (5), $\dot{Z}_2^{(2)}(t+\Delta t)$ from (7) and $\dot{Z}_0^{(2)}(t+\Delta t)$ from (3) using $\{T\}_{t+\Delta t}^{(1)}$.
4. If

$$\left|\frac{\dot{Z}_1^{(2)}(t+\Delta t) - \dot{Z}_1^{(1)}(t+\Delta t)}{\dot{Z}_1^{(1)}(t+\Delta t)}\right| > \delta \quad \text{or} \quad \left|\frac{\dot{Z}_2^{(2)}(t+\Delta t) - \dot{Z}_2^{(1)}(t+\Delta t)}{\dot{Z}_2^{(1)}(t+\Delta t)}\right| > \delta$$

$$\text{or} \quad \left|\frac{\dot{Z}_0^{(2)}(t+\Delta t) - \dot{Z}_0^{(1)}(t+\Delta t)}{\dot{Z}_0^{(1)}(t+\Delta t)}\right| > \delta,$$

where δ is a user tolerance, then choose $q \in [0,1]$, put $\dot{Z}_1^{(1)}(t+\Delta t) = q\dot{Z}_1^{(2)}(t+\Delta t) + (1-q)\dot{Z}_1^{(1)}(t+\Delta t)$, $\dot{Z}_2^{(1)}(t+\Delta t) = q\dot{Z}_2^{(2)}(t+\Delta t) + (1-q)\dot{Z}_2^{(1)}(t+\Delta t)$, $\dot{Z}_0^{(1)}(t+\Delta t) = q\dot{Z}_0^{(2)}(t+\Delta t) + (1-q)\dot{Z}_0^{(1)}(t+\Delta t)$, $Z_1^{(1)}(t+\Delta t) = Z_1(t) + \Delta t\dot{Z}_1^{(1)}(t+\Delta t)$, $Z_2^{(1)}(t+\Delta t) = Z_2(t) + \Delta t\dot{Z}_2^{(1)}(t+\Delta t)$, $Z_0^{(1)}(t+\Delta t) = Z_0(t) + \Delta t\dot{Z}_0^{(1)}(t+\Delta t)$, and go back to Step 2.

Otherwise, put $\{T\}_{t+\Delta t} = \{T\}_{t+\Delta t}^{(1)}$, $\dot{Z}_1(t+\Delta t) = \dot{Z}_1^{(2)}(t+\Delta t)$, $\dot{Z}_2(t+\Delta t) = \dot{Z}_2^{(2)}(t+\Delta t)$, $\dot{Z}_0(t+\Delta t) = \dot{Z}_0^{(2)}(t+\Delta t)$, $Z_1(t+\Delta t) = Z_1(t) + \frac{1}{2}\Delta t[\dot{Z}_1^{(2)}(t+\Delta t) + \dot{Z}_1(t)]$, $Z_2(t+\Delta t) = Z_2(t) + \frac{1}{2}\Delta t[\dot{Z}_2^{(2)}(t+\Delta t) + \dot{Z}_2(t)]$, $Z_0(t+\Delta t) = Z_0(t) + \frac{1}{2}\Delta t[\dot{Z}_0^{(2)}(t+\Delta t) + \dot{Z}_0(t)]$ and go to the next time step.

5 Computational experiments

The pulsed-laser induced phase change processes in the a-Si layers deposited on the quartz substrate were simulated for a XeCl excimer laser (308 nm, 28 ns FWHM). The initial thickness A of the a-Si layer varied from 50 nm to 8000 nm, the laser energy density E was in the range $[0.05\,\mathrm{Jcm^{-2}}, 1.00\,\mathrm{Jcm^{-2}}]$. The thermophysical and optical data for a-Si, pc-Si, l-Si, and quartz necessary for our model were taken from Refs. [7–15].

First, we performed numerical tests of the computational model. We varied the length of finite elements L_i in the individual phases and materials and the maximum allowable time step $\Delta t_{\max}$, and we also tested the influence of the relaxation factor q and of the tolerance δ. Our aim was to find the optimum values of these parameters that would guarantee 0.1% agreement in the characteristic values of the temperature field and the interface positions and velocities as compared with the maximum-accuracy case. The optimum parameters found were $L_{\mathrm{l-Si}} = 0.5\,\mathrm{nm}$, $L_{\mathrm{a-Si}} = 1\,\mathrm{nm}$, $L_{\mathrm{pc-Si}} = 1\,\mathrm{nm}$, $L_s = 20\,\mathrm{nm}$, $\Delta t_{\max} = 1 \times 10^{-3}\,\mathrm{ns}$, $\delta = 10^{-4}$, $q = 0.5$.

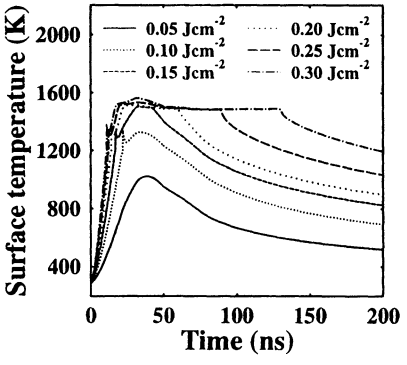

Figure 1a: Time histories of the surface temperatures for $A = 230$ nm.

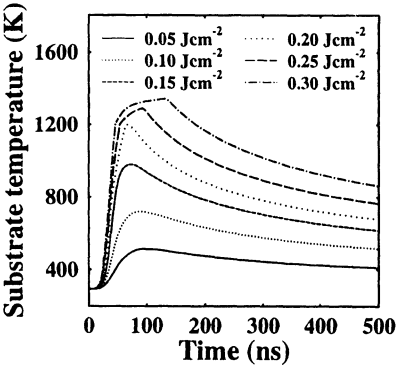

Figure 1b: Time histories of the substrate temperatures for $A = 230$ nm.

Then, we studied the influence of the pulse energy density E. Fig. 1a shows the surface temperature for $A = 230$ nm and lower values of E. The first peak in temperature profiles gives an evidence of solid-state crystallization from the surface which is accompanied by fast release of latent heat. The second maximum corresponds to the maximum power density of the laser pulse. The solid-state crystallization threshold $E_{sc} = 0.10$ Jcm^{-2} and melting threshold $E_m = 0.15$ Jcm^{-2} can also be identified in this figure.

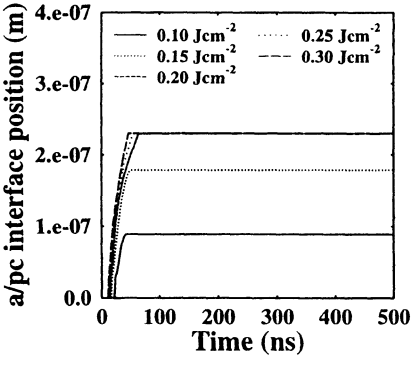

Figure 2a: Position of the a-Si/pc-Si interface for $A = 230$ nm.

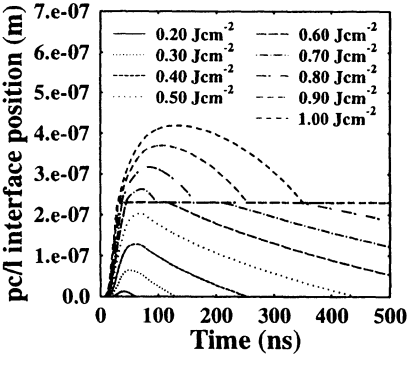

Figure 2b: Position of the pc-Si/l-Si interface for $A = 230$ nm.

In Fig. 1b we present the history of substrate surface temperatures. At $E = 0.20$ Jcm^{-2} the substrate achieves the temperature of a-Si to pc-Si phase transition T_{ac}, and therefore the full 230 nm a-Si layer is crystallized in solid state during the pulse. This is illustrated in Fig. 2a. The quartz

substrate begins to melt at $E = 0.70$ Jcm^{-2} as shown in Fig. 2b.

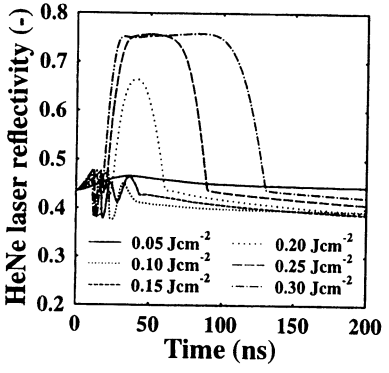

Figure 3a: HeNe laser reflectivity for $A = 230$ nm.

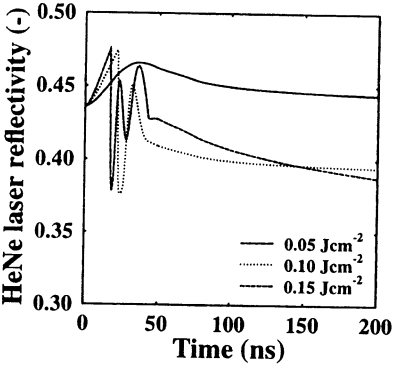

Figure 3b: HeNe laser reflectivity for $A = 230$ nm, a detail.

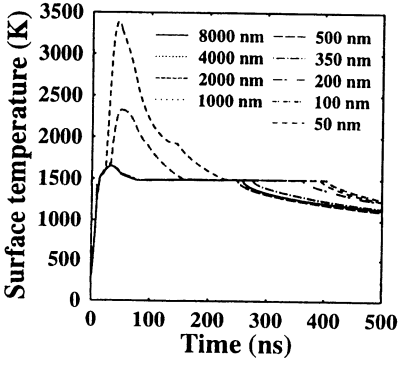

Figure 4a: Time histories of the surface temperatures for $E = 0.45$ J/cm^2.

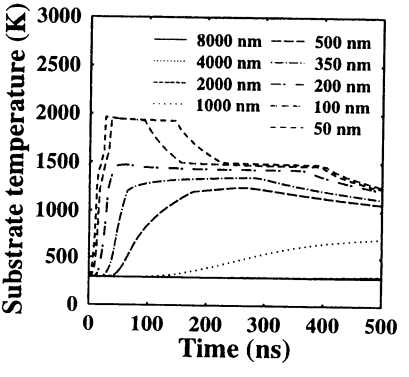

Figure 4b: Time histories of the substrate temperatures for $E = 0.45$ J/cm^2.

The computational analogs to the time-resolved reflectivity measurements (TRR), which belong to standard experimental techniques (see [3]) and consist in monitoring the reflectivity of probe cw laser (e.g. the HeNe laser) as a function of time, are presented in Fig. 3a and, in detail, in Fig. 3b. Apparently, the initial oscillations are a consequence of the pc-Si layer appearance and growth that result in significant changes of optical properties of the system. The system is strongly optically nonhomogeneous since the complex refraction index depends on temperature and also undergoes jump changes at the interfaces between the particular layers.

In the final set of computational experiments we investigated the influence of the initial thickness of the a-Si layer $A \in [50\text{ nm}, 8000\text{ nm}]$ for $E = 0.45\ \text{Jcm}^{-2}$. Figs. 4a,b show that the surface and substrate temperature maxima decrease with increasing the a-Si layer thickness A. This is a consequence of the fact that for $A < 150$ nm, the quartz substrate melts. The latent heat of melting of quartz is approximately 6–7 times lower compared to that of pc-Si, and therefore the melt front propagates faster and deeper into the quartz layer. This is documented in Fig. 5a.

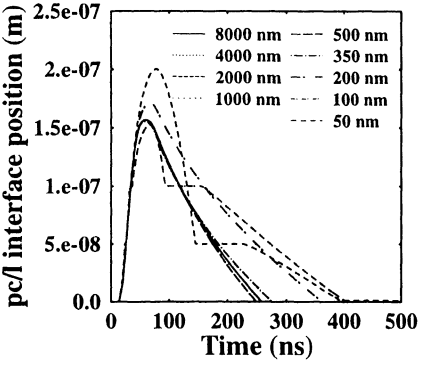

Figure 5a: Position of the pc-Si/l-Si interface for $E = 0.45\ \text{J/cm}^2$.

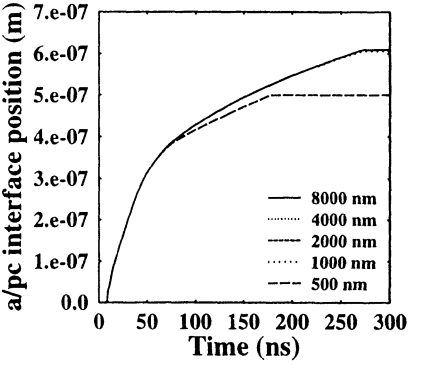

Figure 5b: Position of the a-Si/pc-Si interface for $E = 0.45\ \text{J/cm}^2$.

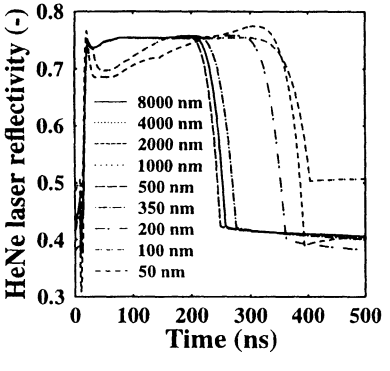

Figure 6a: HeNe laser reflectivity for $E = 0.45\ \text{J/cm}^2$.

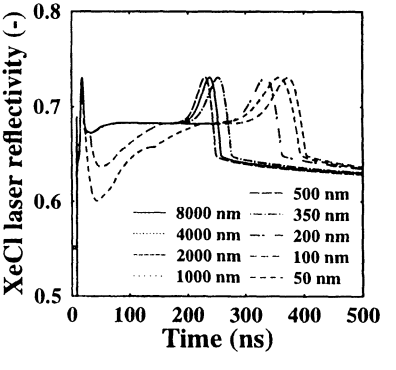

Figure 6b: XeCl laser reflectivity for $E = 0.45\ \text{J/cm}^2$.

For $A > 2000$ nm the substrate temperature is basically unaffected by the laser pulse and all processes take place in the a-Si layer. Fig. 5b illustrates the physical reason of this fact. We can see here that for $A > 500$ nm the

solid-state crystallization ends before reaching the substrate surface. The latent heat release deep inside the a-Si layer then stops and deeper layers are heated only by heat conduction which is, moreover, slower in a-Si and quartz than in pc-Si.

Figs. 6a,b show the time evolution of reflectivities of the probe HeNe laser and the incident XeCl laser, which illustrates well the physical phenomena described before. The significant decrease in both HeNe and XeCl reflectivities for $A \leq 100$ nm after the second peak corresponding to the appearance of the liquid phase is an apparent consequence of the fast temperature increase (see Fig. 4a) after the moment when the melt front moves into the quartz substrate.

6 Conclusions

The computational simulations show that there are no significant changes in the behavior of the system for the initial thickness A of the a-Si layer above a certain limit depending on the energy density of the pulse. However, for lower values of A, when the melt front enters the substrate, the lower latent heat of melting of quartz causes a fast increase of the surface temperatures. The initial oscillations in the HeNe laser reflectivity observed experimentally by another authors in the time-resolved reflectivity measurements [4], which are due to the a-Si to pc-Si phase transition, are reproduced by the model successfully. It can be noticed that the model can be used with advantage to estimate the values of both thermophysical and optical parameters of pc-Si depending on the grain size, which have not been determined experimentally until now.

Acknowledgement

This paper is based upon work supported by the Grant Agency of the Czech Republic, under grant # 202/93/2383.

References

1. Kamins, T.I. *Polycrystalline Silicon for Integrated Circuits Applications*, Kluwer Academic, Boston, 1988.

2. Thompson, M.O., Galvin, G.J., Mayer, J.W., Peercy, P.S., Poate, J.M., Jacobson, D.C., Cullis, A.G. Chew, N.G. Melting temperature and explosive crystallization of amorphous silicon during pulsed laser irradiation, *Phys. Rev. Lett.*, 1984, **52**, 2360–2363.

3. Lowndes, D.H., Pennycook, S.J., Jellison, G.E., Withrow, S.P., Mashburn, D.N. Solidification of highly undercooled liquid silicon produced by pulsed laser melting of ion-implanted amorphous silicon: time-resolved and microstructural studies, *J. Mater. Res.*, 1987, **2**, 648–680.

4. Im, J.S., Kim, H.J., Thompson, M.O. Phase transformation mechanisms involved in excimer laser crystallization of amorphous silicon films, *Appl. Phys. Lett.*, 1993, **63**, 1969–1971.
5. Sameshima, T., Usui, S. Pulsed laser induced amorphization of silicon films, *J. Appl. Phys.*, 1991, **70**, 1281–1289.
6. Černý, R., Přikryl, P. Computational solution of a moving boundary problem with two phase interfaces, *ZAMM*, 1994, **74**, 568–570.
7. Ulrych, I., El-Kader, K.M.A., Cháb, V., Kočka, J., Přikryl, P., Vydra, V., Černý, R. Properties of recrystallized amorphous silicon prepared by XeCl excimer laser irradiation, *Mat. Sci. Forum*, 1995, **173-174**, 29–34.
8. Webber, H.C., Cullis, A.G., Chew, N.G. Computer simulation of high speed melting of amorphous silicon, *Appl. Phys. Lett.* , 1983, **43**, 669–671.
9. Wood, R.F., Jellison, G.E. Melting model of pulsed laser processing, Chapter 4, *Semiconductors and Semimetals*, eds. R.F. Wood, C,W. White, R.T. Young, Vol. 23, pp. 165–250, Academic Press, New York, 1984.
10. Stolk, P.A., Saris, F.W., Berntsen A.J.M., van der Weg, W.F., Sealy, L.T., Barklie, R.C., Krötz, G., Müller, G. Contribution of defects to electronic, structural, and thermodynamic properties of amorphous silicon, *J. Appl. Phys.*, 1994, **75**, 7266–7286.
11. Lowndes, D.H., Jellison, G.E., Pennycook, S.J., Withrow, S.P., Mashburn, D.N. Direct measurements of the velocity and thickness of explosively propagating buried molten layers in amorphous silicon, *Appl. Phys. Lett.*, 1986, **48**, 1389–1391.
12. de Unamuno, S., Fogarassy, E. A thermal description of the melting of c- and a-silicon under pulsed excimer lasers, *Appl. Surf. Sci.*, 1989, **36**, 1–11.
13. Glassbrenner, C.J., Slack, G.A. Thermal conductivity of silicon and germanium from 3 K to the melting point, *Phys. Rev.*, 1964, **134**, A1058–A1069.
14. Desai, P.D. Thermodynamic properties of iron and silicon, *J. Phys. Chem. Ref. Data*, 1986, **15**, 976–983.
15. Lide, D.R. (ed.). *CRC Handbook of Chemistry and Physics*, 72th ed., CRC Press, Boca Raton, 1991.